Wiley
International Journal of RF and Microwave Computer-Aided Engineering
Volume 2024, Article ID 3884672, 12 pages
https://doi.org/10.1155/2024/3884672

WILEY

Research Article

Stub Asymmetry-Enabled Self-Phase-Shift Circularly Polarized Antenna under Dual-Mode Resonance

Shan-Shan Gu,[1] **Wen-Jun Lu**,[1] **Fei-Yan Ji**,[1] **and Lei Zhu**[2]

[1]*Nanjing University of Posts and Telecommunications, Nanjing 210003, China*
[2]*University of Macau, Macau 999078, China*

Correspondence should be addressed to Wen-Jun Lu; wjlu@njupt.edu.cn

Received 17 January 2024; Revised 30 April 2024; Accepted 9 May 2024; Published 24 May 2024

Academic Editor: Chow-Yen-Desmond Sim

In this article, a novel design approach to wideband dual-mode resonant circularly polarized (CP) antenna is advanced. An analytical design approach with low complexity as supported by a set of closed-form formulas is presented. Thus, the wideband dual-mode CP characteristics can be forward predicted and simply realized by incorporating stub asymmetry-enabled self-phase-shift dipoles and unequal feeding branches. At first, stubs are employed to broaden the impedance bandwidth by simultaneously exciting dual resonant modes. Then, the phase quadrature and equal magnitude conditions for wideband CP can be automatically realized by incorporating unequal Y-shaped microstrip branches and asymmetric slotline stubs. Finally, the coincidence between the simulated and measured results of the fabricated prototype antenna further confirms the feasibility of the design approach. It is shown that the presented antenna can exhibit an impedance bandwidth of 20.1% and a 3 dB axial ratio bandwidth of 16.3% in the boresight direction.

1. Introduction

Basically, there are two distinctive ways to introduce 90° phase quadrature in circularly polarized (CP) antenna designs [1–4]: One is the single-port fed, self-phase quadrature technique [1–3], which uses the current path difference of a pair of orthogonal, equal amplitude excited dipoles to yield 90° phase quadrature. Another one is the dual-port fed [4] technique which relies on an external directional coupler with equal amplitude and 90° phase quadrature. Inherently, both design approaches may yield narrowband characteristics, with impedance bandwidth of about 4% and 3 dB axial ratio (AR) bandwidth of about 3%, respectively.

Recent years, a considerable number of wideband broadening design approaches have been proposed. On the basis of their distinctive operation mechanisms, these wideband CP antennas can be classified into five different categories. As is well known, traveling-wave and leaky-wave antennas can naturally yield wide bandwidths owing to their radiation characteristics [5–8]. Alternatively, complementary dipole [9–11] configurations can also be used to yield broadband designs. By introducing several orthogonal placed perturbed elements, i.e., strips [9], stubs [10], or external pins [11], multiple resonant modes have been excited to effectively expand the CP bandwidths. Sequentially rotated dipole configurations are known as the third type of broadband CP antennas [12–17]. In those ways, the 90° phase differences have been satisfied by utilizing two paired perpendicular crossed dipoles to yield wide CP bandwidths. Broadband CP antennas have been developed based upon dielectric resonator configurations [18, 19] and ring slot configurations [20, 21] in recent years. The wideband CP radiation characteristics with equal magnitude and phase-in-quadrature conditions can be realized by combining external complicated feed networks [19] or parasitic elements [21]. In general, most of the aforementioned CP antennas exhibit wide impedance bandwidths, while their AR bandwidths are relatively narrower than the impedance ones. Among them, it is necessary to introduce additional several parasitic radiators [11, 20, 21] or incorporate external 90-degree phase shifters [15], thereby increasing the design complexity. Wideband CP antennas with multimode resonant AR bandwidths

[22–25] have recently drawn more and more attentions. Filtering feeding networks can be codesigned with CP patch antennas [26, 27] at the cost of enlarged area or more occupied footprint. Incorporating a multimode resonant dipole [28] can also simultaneously broaden the impedance as well as the AR bandwidths of planar end-fire CP antennas (PECPAs) [29, 30]. Therefore, it is always a challenging task to design wideband CP antennas while simultaneously attaining wide impedance and 3 dB AR bandwidths, simple configuration.

In this article, an analytical design approach to wideband dual-mode resonant open-end CP slotline antenna is advanced. Unlike traditional design approaches which rely on external phase shift networks/parasitic elements [22–30], the prototype antenna with enhanced impedance and 3 dB AR bandwidths can be forward predicted and simply implemented by incorporating stub asymmetry-enabled self-phase-shift dipoles and unequal feeding branches. In this case, equal magnitude and phase-in-quadrature conditions can be automatically satisfied to yield dual-mode resonant CP bandwidths. As fabricated and measured, the proposed CP antenna with nearly equal broadband impedance and 3 dB AR bandwidths (meaning 20.1% and 16.3%) can be obtained while maintaining a simplest wideband design with equal length, straight-line configuration of the orthogonal principal slotline radiators.

2. Antenna Configuration and Design Procedure

The design process of wideband open-end slotline antenna under dual-mode resonance stems from the simplest, straight narrowband slotline dipole, as illustrated in Figure 1. By employing a set of closed-form formulas, the bandwidth broadening mechanism of the proposed antenna can be forward theoretically predicted. Accordingly, stub asymmetry-enabled self-phase-shift dipoles and unequal microstrip line (MSL) branches are combined perpendicularly in design for the wideband dual-mode resonant CP characteristics. The consequent key parameters are then analyzed in detail. A two-step design process is presented to illustrate the operational principle as well as design approach. Herein, the proposed antenna is designed on a substrate with relative permittivity of $\varepsilon_r = 2.65$ and thickness of $h = 1$ mm.

2.1. Dual-Mode Resonant Design Approach. The first step is to excite and perturb the 1.5-wavelength resonant mode by incorporating a slotline stub at its surface E-field's node of the open-end slotline antenna ($W << L$), as illustrated in Figure 1(a). As is revealed in [31–33], the 1.5-wavelength resonant mode can be tuned downward its fundamental counterpart to yield wideband operation with two resonances. For further verification, two identical half-wavelength slotline dipoles with perturbed stubs, namely, dipole 1 and dipole 2, are both etched out on the metallic ground, as shown in Figure 1(b). The length $L_{s(1,2)}$, the width W_s, and the offset distance $D_{s(1,2)}$ of the slotline stubs are empirically determined by using

$$L_s \approx \frac{\lambda_g}{4},$$
$$W_s \approx \frac{\lambda_g}{20}, \quad (1)$$
$$D_s \approx \frac{\lambda_g}{3},$$

where λ_g is the guided wavelength in the substrate [31]. Then, the values of these sizes can be readily chosen as $L_{s(1,2)} = 20.5$ mm, $W_s = 3.0$ mm, and $D_{s(1,2)} = 29.5$ mm. Herein, the microstrip lines of the dipoles are designed to terminate to be short-circuited (S.C.) as shown in the left side of Figure 1(b) and open-circuited (O.C.) with a 1/4-wavelength extension as shown in the right side of Figure 1(b), respectively. As presented in previously research [22, 34], the microstrip lines should be placed near the short end of slotlines with the dimension of $D_f = 3.5$ mm. Ideally, each dipole should exhibit an input impedance of 100 Ω (i.e., $W_{fy} = 0.8$ mm) [35], so that the in-parallel input impedance at the microstrip T-junction would be 50 Ω that could be directly matched to the instrument.

In order to intuitively observe the impendence bandwidth broadening mechanism, the impedance frequency response curves on the Smith chart of the slotline dipoles with unloaded/loaded stubs are illustrated in Figure 1(c). Compared to the unloaded case, when a pair of the bilateral stubs is incorporated, the resultant trace of the circled impedance can be concentrated into a circle on the Smith chart. The resultant results indicate that dual resonant modes can be indeed simultaneously excited by employing the slotline stubs, thereby further broadening the impedance bandwidth. In addition, both two orthogonal dipoles with different forms of microstrip line terminals exhibit quite similar, average input impedance of about 75 to 100 Ω. Therefore, for the sake of design simplification and more degrees of freedom, each branch of the microstrip lines is employed open-circuited stubs.

Hence, as shown in Figure 1(d), the geometry of the open-end slotline CP antenna can be obtained by connecting two orthogonal dipoles in parallel, with key parameters indicated. As can be observed, the proposed antenna consists of a ground plane etched with a pair of the orthogonal, identical half-wavelength open-end stub-loaded slotline radiators, a dielectric substrate, and a Y-shaped centre-fed microstrip line. The width of the main feedline, i.e., $W_f = 2.8$ mm, is calculated by employing the microstrip line design formula presented in the classical antenna handbook [34]. In this case, the proposed wideband CP antenna can be realized by combining the two stub-loaded slotlines and a microstrip-fed line with unequal branches: equal magnitude and phase-in-quadrature conditions can be realized by incorporating identical radiating dipoles and unequal Y-shaped MSL branches.

2.2. 3 dB AR Bandwidth Enhancement. The second step is to incorporate unequal Y-shaped microstrip branches (L_{f1}, L_{f2}) and asymmetric bilateral stubs (L_{s1}, D_{s1}; L_{s2}, D_{s2}) to

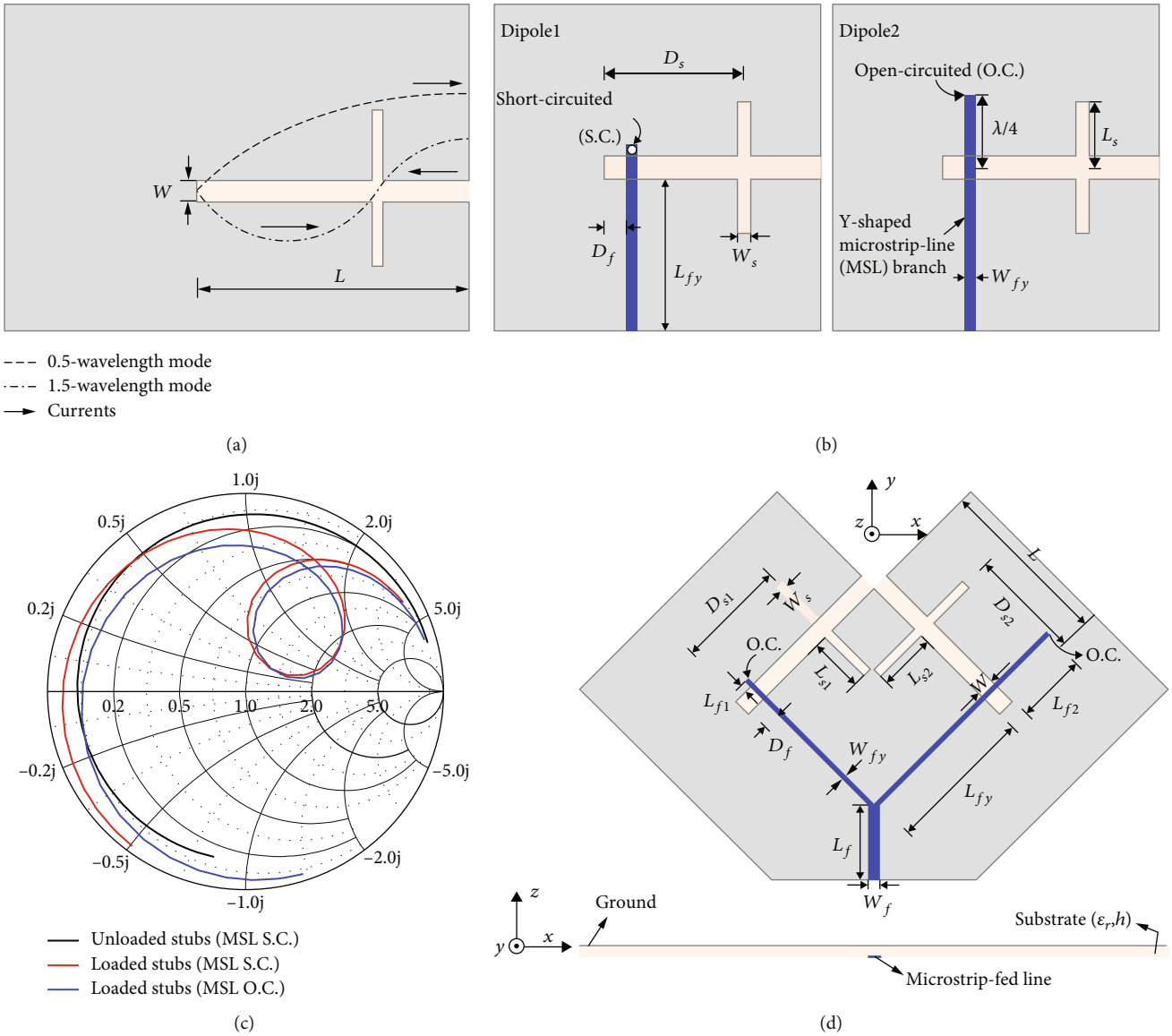

FIGURE 1: Open-end slotline dipoles: (a) E-field distributions, (b) the microstrip line terminals to be short-circuited (S.C.) and open-circuited (O.C.) with a 1/4-wavelength extension, (c) Smith chart with unloaded/loaded stubs ($L = 50.5$ mm, $W = 5$ mm, $D_s = 29.5$ mm, $L_s = 25.5$ mm, $W_s = 3$ mm, $D_f = 3.5$ mm, $W_{fy} = 0.8$ mm, and $L_{fy} = 47$ mm), and (d) geometry of the proposed CP antenna.

automatically meet equal magnitude and phase-in-quadrature conditions for wideband CP radiation. Ideally, suppose that two identical dipoles be effectively excited with equal magnitude. If the 90° phase difference can be satisfied by incorporating a suitable length difference $\Delta L_f = L_{f2} - L_{f1}$, the CP characteristic will be implemented in the boresight direction. As illustrated in [29] and [36], L_{f1}, L_{f2}, and ΔL_f can be approximately estimated and determined to be 5.0 mm, 25.5 mm, and 20.5 mm by using the following equations:

$$L_{f1} \approx \frac{\lambda_g}{20}, \qquad L_{f2} \approx \frac{\lambda_g}{4}, \tag{2a}$$

$$\Delta L_f = L_{f2} - L_{f1} \approx \frac{\lambda_g}{5}. \tag{2b}$$

In the case of loading symmetric slotline stubs, i.e., $L_{s(1,2)} = 18.5$ mm, $W_s = 3.0$ mm, and $D_{s(1,2)} = 29.5$ mm, the effects of L_{f1} on the reflection coefficient and 3 dB AR are plotted in Figures 2(a) and 2(b), respectively. Under those circumstances, the proposed antenna has a wide impedance bandwidth but a narrow 3 dB AR bandwidth. Fortunately, it should be potential to yield a wide 3 dB AR bandwidth. For better illustration, the first two odd-order resonant modes are named as mode 1 and mode 2, respectively. As can be seen, with the increase of L_{f1}, a better impedance matching of the proposed antenna is achieved while the tendency of wider 3 dB AR bandwidth is deteriorated. Furthermore, when L_{f1}

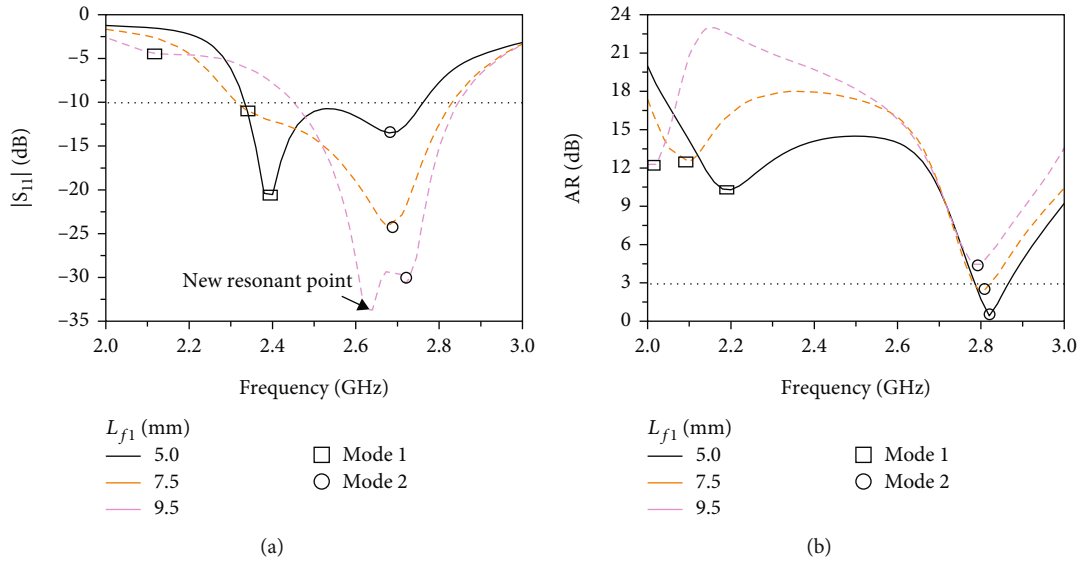

FIGURE 2: Parametric studies and comparisons of L_{f1} by loading symmetric slotline stubs: (a) $|S_{11}|$ and (b) AR ($L = 50.5$ mm, $W = 5.0$ mm, $W_s = 3$ mm, $D_s = 29.5$ mm, $L_s = 18.5$ mm, $L_{fy} = 47.0$ mm, $L_{f2} = 25.5$ mm, $W_f = 2.8$ mm, $W_{fy} = 0.8$ mm, $D_f = 3.5$ mm, and $L_f = 22.7$ mm).

increases, the resonant frequencies of mode 1 of 3 dB AR are progressively moved down while the ones of mode 2 have barely any influence. The resultant phenomenon also applies to the cases of $|S_{11}|$ frequency responses. In particular, when $L_{f1} = 9.5$ mm, which is about 1/10 wavelength, a new resonant frequency appears near the third-order mode [36]. As is indicated, the better CP performance can be obtained when $L_{f1} = 5$ mm ($\Delta L_f = 20.5$ mm), which falls precisely within the predicted range by Equations (2a) and (2b).

According to the above-mentioned analysis, asymmetric bilateral stubs are additionally introduced to achieve dual-mode resonant CP bandwidths. Simultaneously, a set of closed-form formulas are employed to predict the bandwidth broadening mechanism through forward modelling. Here, we will elaborate on the operating principle in detail: for two asymmetrically perturbed stubs, if the length difference $\Delta L_s = L_{s1} - L_{s2}$ can satisfy the condition in Equations (3a) and (3b), the discontinuities along the stubs' direction will be compensated. Similarly, the discontinuities along the dipoles' direction can be compensated by $\Delta D_s = D_{s2} - D_{s1}$ using Equations (4a) and (4b). As a result, equal magnitude and phase-in-quadrature conditions can be automatically satisfied to yield dual-mode resonance on AR frequency response towards broadening the AR and impedance bandwidths in final. Drawing support from Equations (3a), (3b), (4a), and (4b) and defined variables, the initial dimensions of these sensitive parameters can be derived as $L_{s1} = 21.5$ mm, $L_{s2} = 20.0$ mm, $\Delta L_s = 1.5$ mm, $D_{s1} = 27.0$ mm, $D_{s2} = 30.0$ mm, and $\Delta D_s = 3.0$ mm, respectively.

$$L_{s1} \approx \frac{\lambda_g}{6} + \frac{\Delta L_s}{2}, \quad L_{s2} \approx \frac{\lambda_g}{6} - \frac{\Delta L_s}{2}, \tag{3a}$$

$$\Delta L_s = L_{s1} - L_{s2} \approx \frac{\lambda_g}{40}, \tag{3b}$$

$$D_{s1} \approx \frac{\lambda_g}{3} - \frac{\Delta D_s}{2}, \quad D_{s2} \approx \frac{\lambda_g}{3} + \frac{\Delta D_s}{2}, \tag{4a}$$

$$\Delta D_s = D_{s2} - D_{s1} \approx \frac{\lambda_g}{20}. \tag{4b}$$

Both compensated and uncompensated magnitude and phase unbalances of asymmetric stubs (L_{s1}, D_{s1}; L_{s2}, D_{s2}) and symmetric stubs (L_s, D_s) in the boresight direction have been numerically studied in Figure 3. As is compared and indicated, incorporating the asymmetric stubs may yield both wideband equal magnitude and phase-in-quadrature frequency responses: the magnitude unbalance has been satisfactorily compensated to less than 1 dB, against the uncompensated case of 4.5 dB within the impedance bandwidth (i.e., 2.35-2.65 GHz). Simultaneously, the phase difference can be compensated from ±30° to less than −10° accordingly, whereupon $D_{s1} = 27.0$ mm, $L_{s1} = 21.5$ mm, $D_{s2} = 29.5$ mm, and $L_{s2} = 20.5$ mm. As is observed, LHCP radiation can be attained in the boresight direction. If right-handed CP (RHCP) is required, the positions of the unequal branches and asymmetric stubs should be interchanged.

2.3. Parametric Studies. For more details, a series of parametric studies on ΔL_s, ΔD_s, L_{s1}, L_{s2}, D_{s1}, D_{s2}, L_{f2}, and D_f are in progress to validate the precision of the prediction Equations (3a), (3b), (4a), and (4b) by employing the HFSS simulator. For convenience, the sensitive antenna parameters are distinctively investigated under the condition that all other parameters keep unchanged. Figure 4 illustrates

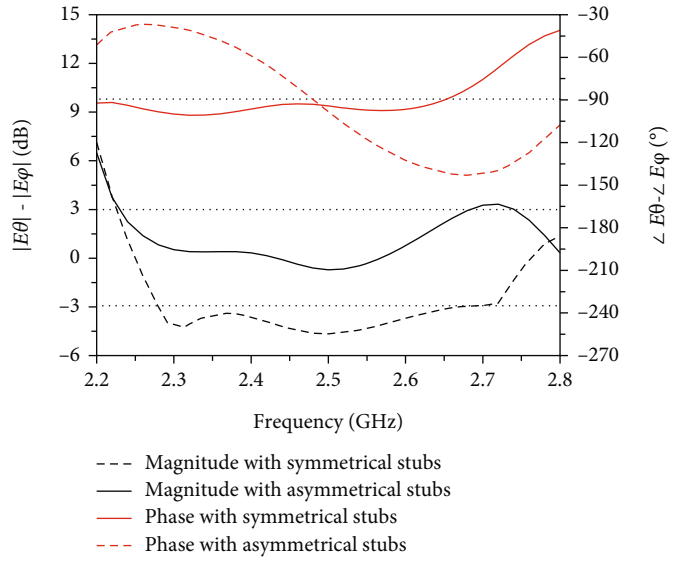

FIGURE 3: Compensated and uncompensated E-field magnitude and phase unbalance conditions with asymmetrical and symmetrical stubs.

the parametric studies and comparisons of asymmetric stubs on the reflection coefficients and axial ratios. As is seen in Figures 4(a) and 4(b), changing the asymmetry in just one direction, i.e., $\Delta L_s = 0$ mm or $\Delta D_s = 0$ mm, cannot automatically excite the conditions of equal magnitude and phase-in-quadrature. As shown in Figures 4(c) and 4(d), it is apparent that increasing D_{s1} can significantly widen the bandwidth of AR < 3 dB. To be more explicit, the left minima in the AR response is consequently controlled by D_{s1}: larger D_{s1} may yield lower left minima AR frequency point. The change in D_{s1} has little impact on the right minima one. It is the exact opposite of the relationship between D_{s2} and two minima AR frequency points: smaller D_{s2} may cause the right minima frequency point to shift towards higher frequency but rarely affect the left one, thus leading to a wider 3 dB bandwidth. These conclusions are also applicable in the cases of $|S_{11}|$ frequency responses. Figures 4(e) and 4(f) indicate that the dual-resonant wideband performance is sensitive to the length of L_{s2}, while less sensitive to the length of L_{s1}. As such, the values of L_{s1} and L_{s2} accurately fall within the range as predicted by Equations (4a) and (4b). According to the simulated results, as graphically illustrated in Figures 4(c), 4(d), 4(e), and 4(f), it can be concluded from the procedure above that when $D_{s1} = 27.0$ mm and $D_{s2} = 29.5$ mm as well as $L_{s1} = 21.5$ mm and $L_{s2} = 20.5$ mm, i.e., $\Delta D_s = 2.5$ mm and $\Delta L_s = 1.0$ mm, nearly equal broad bandwidths of impedance and AR characteristics can be achieved. Hence, the numerically simulated results are consistent with the ones predicted by Equations (3a), (3b), (4a), and (4b), with the discrepancies less than 10%.

For better impedance and 3 dB AR bandwidths simultaneously in the broadside direction, the effects of L_{f2} and D_f are further studied and shown in Figures 4(g) and 4(h). It can be observed that slightly smaller L_{f2} and larger D_f can obtain wider impedance and 3 dB AR bandwidths; thus, L_{f2} and D_f are numerically determined as 25.5 mm and 3.5 mm, respectively. As is shown, the enhanced wideband 3 dB AR and impedance bandwidths can be achieved by incorporating asymmetric slotline stubs and unequal Y-shaped microstrip branches. So far, all of the key parameters of the proposed antenna have been determined and studied in a step-by-step manner. The initial and simulated parameters are tabulated in Table 1. By comparing the empirical formulas as well as parametric studies, a modified formula of Equation (5) for yielding 90° phase quadrature condition for wideband 3 dB AR performance can be attained.

$$\Delta L_f + \Delta L_s + \Delta D_s + \frac{h}{2} \approx \frac{\lambda_g}{4}. \quad (5)$$

3. Numerical and Experimental Validations

For further validating the generality of the proposed design approach, the prototype antenna is fabricated, and the experimental results are compared with the simulated ones in this section. Herein, Figure 5 shows the printed prototype on a modified Teflon substrate with $h = 1$ mm, $\varepsilon_r = 2.65$, and loss tangent $\tan\delta = 0.002$. Figure 6 plots the surface current distributions at 2.68 GHz. At $\omega t = 0°$, the predominant surface current flows in $\theta = 90°$ and $\varphi = 45°$ direction. When $\omega t = 90°$, a dominant current flowing in $\theta = 90°$ and $\varphi = -45°$ direction is observed. It can be observed that the surface current distribution at $\omega t = 180°$ (270°) is equal in magnitude and opposite in phase of that of $\omega t = 0°$ (90°). As the time changes, the surface currents located at the azimuth angle turn in the clockwise direction. It is clearly seen that the proposed antenna can generate a LHCP wave in $+z$-direction. Interchanged dipoles may yield RHCP in $+z$-direction. The prototype antenna's reflection coefficient and radiation characteristics are measured by serving Agilent's N5230A vector network analyzer and Satimo's StarLab near-field antenna measurement system, respectively.

Figure 7 plots the frequency responses of the measured and simulated -10 dB reflection coefficients and axial ratios.

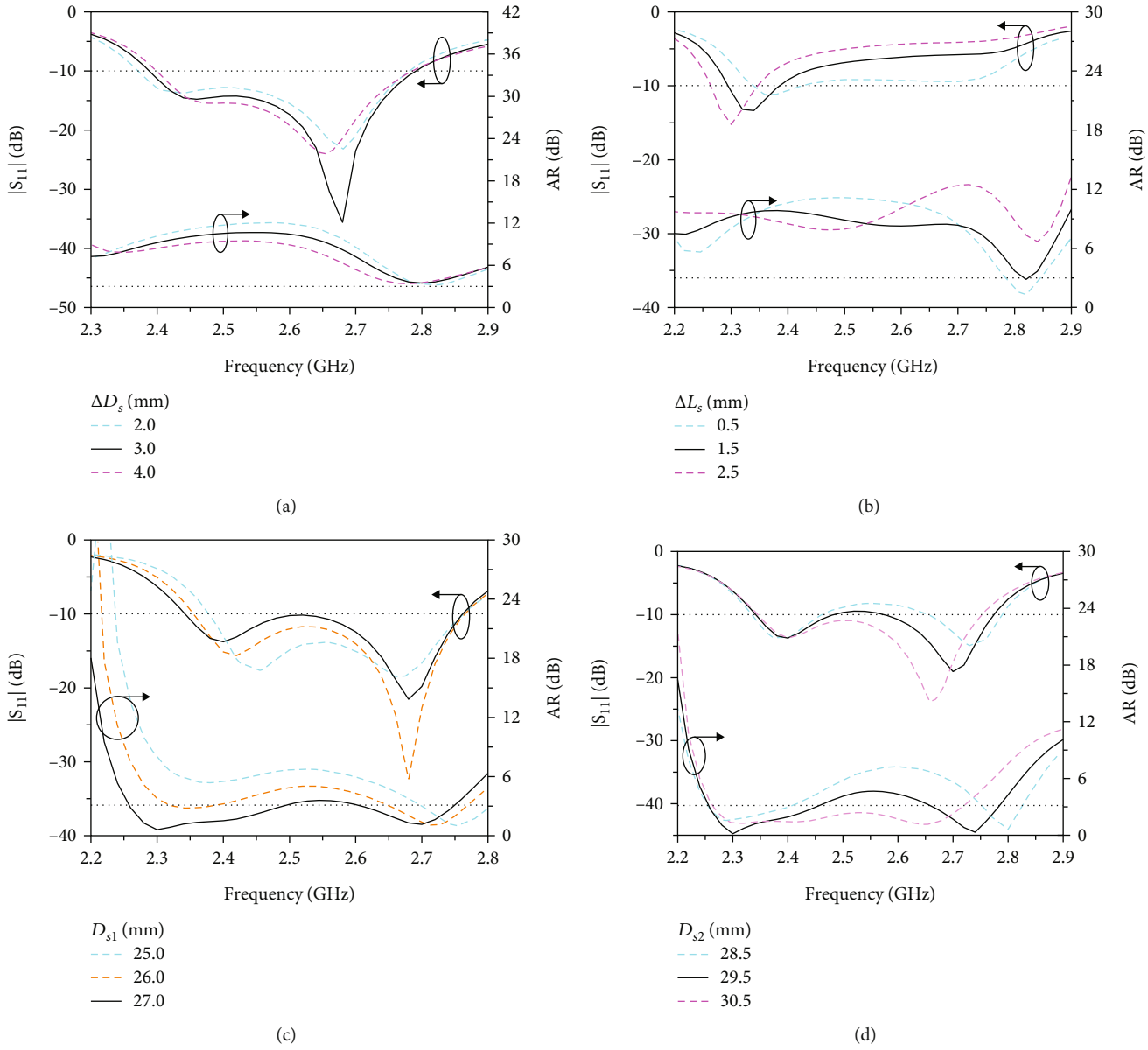

FIGURE 4: Continued.

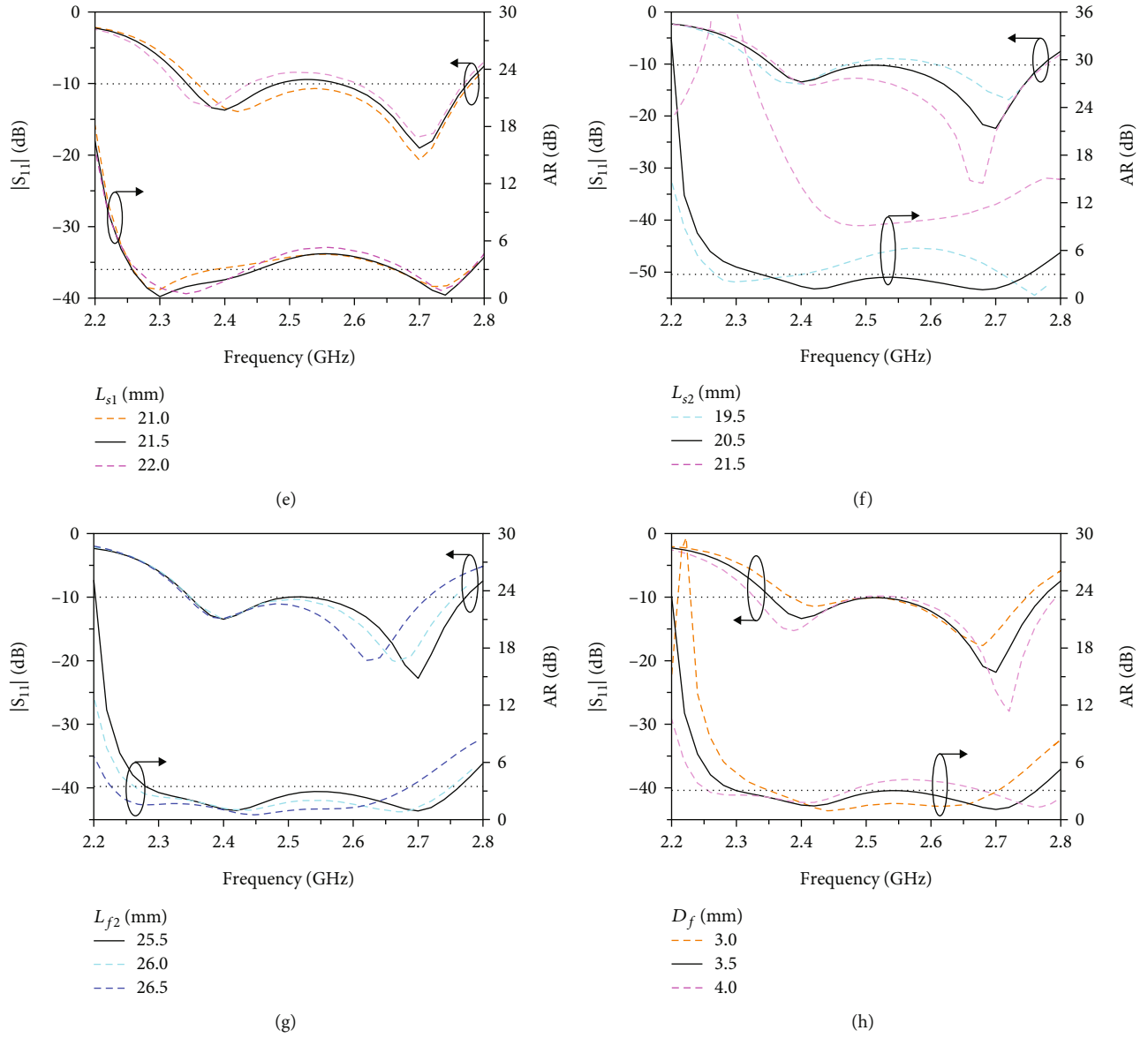

Figure 4: Parametric studies and comparisons of asymmetric stubs: (a) ΔD_s ($\Delta L_s = 0$ mm, $L_{s(1,2)} = 18.5$ mm, and $D_{s(1,2)} = 29.5$ mm), (b) ΔL_s ($\Delta D_s = 0$ mm, $L_s = 18.5$ mm, and $D_s = 29.5$ mm), (c) D_{s1} ($D_{s2} = 30.0$ mm, $L_{s1} = 21.5$ mm, $L_{s2} = 20.0$ mm, and $\Delta L_s = 1.5$ mm), (d) D_{s2} ($D_{s1} = 27.0$ mm, $L_{s1} = 21.5$ mm, $L_{s2} = 20.0$ mm, and $\Delta L_s = 1.5$ mm), (e) L_{s1} ($L_{s2} = 20.0$ mm, $D_{s1} = 27.0$ mm, $D_{s2} = 29.5$ mm, and $\Delta D_s = 2.5$ mm), (f) L_{s2} ($L_{s1} = 21.5$ mm, $D_{s1} = 27.0$ mm, $D_{s2} = 29.5$ mm, and $\Delta D_s = 2.5$ mm), (g) L_{f2} ($L = 50.5$ mm, $W = 5.0$ mm, $W_s = 2.5$ mm, $D_{s1} = 27.0$ mm, $L_{s1} = 21.5$ mm, $D_{s2} = 29.5$ mm, $L_{s2} = 20.5$ mm, $L_{f1} = 5.0$ mm, $D_f = 3.5$ mm, $L_{fy} = 47.0$ mm, $W_{fy} = 0.8$ mm, $L_f = 22.7$ mm, and $W_f = 2.8$ mm), and (h) D_f ($L = 50.5$ mm, $W = 5.0$ mm, $W_s = 2.5$ mm, $D_{s1} = 27.0$ mm, $L_{s1} = 21.5$ mm, $D_{s2} = 29.5$ mm, $L_{s2} = 20.5$ mm, $L_{f1} = 5.0$ mm, $L_{f2} = 25.5$ mm, $L_{fy} = 47.0$ mm, $W_{fy} = 0.8$ mm, $L_f = 22.7$ mm, and $W_f = 2.8$ mm).

Table 1: Antenna parameters (unit: mm).

Parameters	L	W	L_{s1}	L_{s2}	ΔL_s	W_s	L_f	W_f
Initial	50.5	5.0	21.5	20.0	1.5	2.5	22.7	2.8
Simulated	50.5	5.0	21.5	20.5	1.0	2.5	22.7	2.8
Parameters	D_{s1}	D_{s2}	ΔD_s	D_f	L_{fy}	W_{fy}	L_{f1}/L_{f2}	ΔD_f
Initial	27.0	30.0	3.0	3.5	47.0	0.8	5.0/25.5	20.5
Simulated	27.0	29.5	2.5	3.5	47.0	0.8	5.0/25.5	20.5

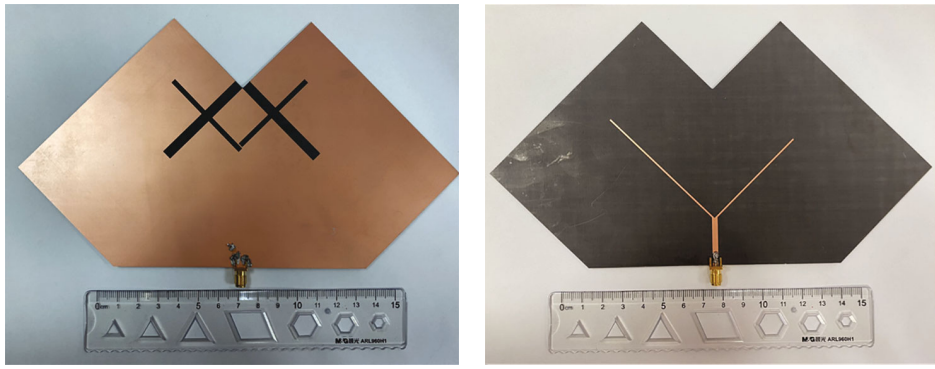

(a) (b)

Figure 5: Photographs of the fabricated prototype: (a) top view and (b) bottom view.

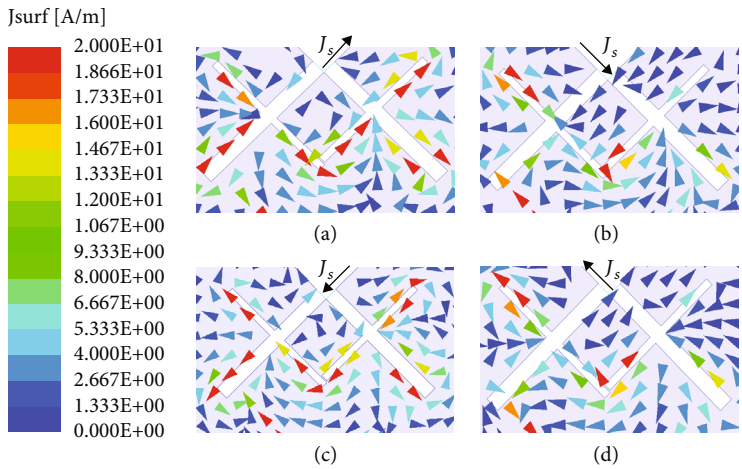

Figure 6: The surface current distributions at 2.68 GHz: (a) $\omega t = 0°$, (b) $\omega t = 90°$, (c) $\omega t = 180°$, and (d) $\omega t = 270°$.

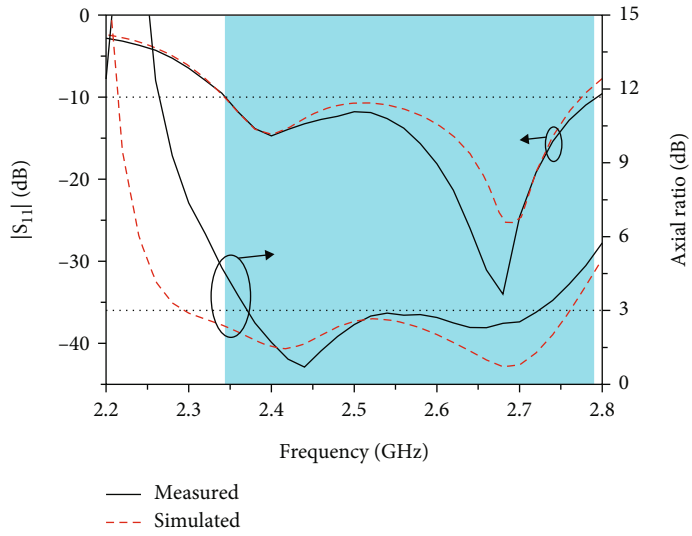

Figure 7: Measured and simulated reflection coefficients and axial ratios.

As is seen, the experimental results have been reasonably well with the numerical ones. Especially, both measured and simulated reflection coefficients and axial ratios appear dual-mode resonant performances as predicted in the theory before, respectively. The measured fundamental resonant frequency is 2.40 GHz, which is very in agreement with the

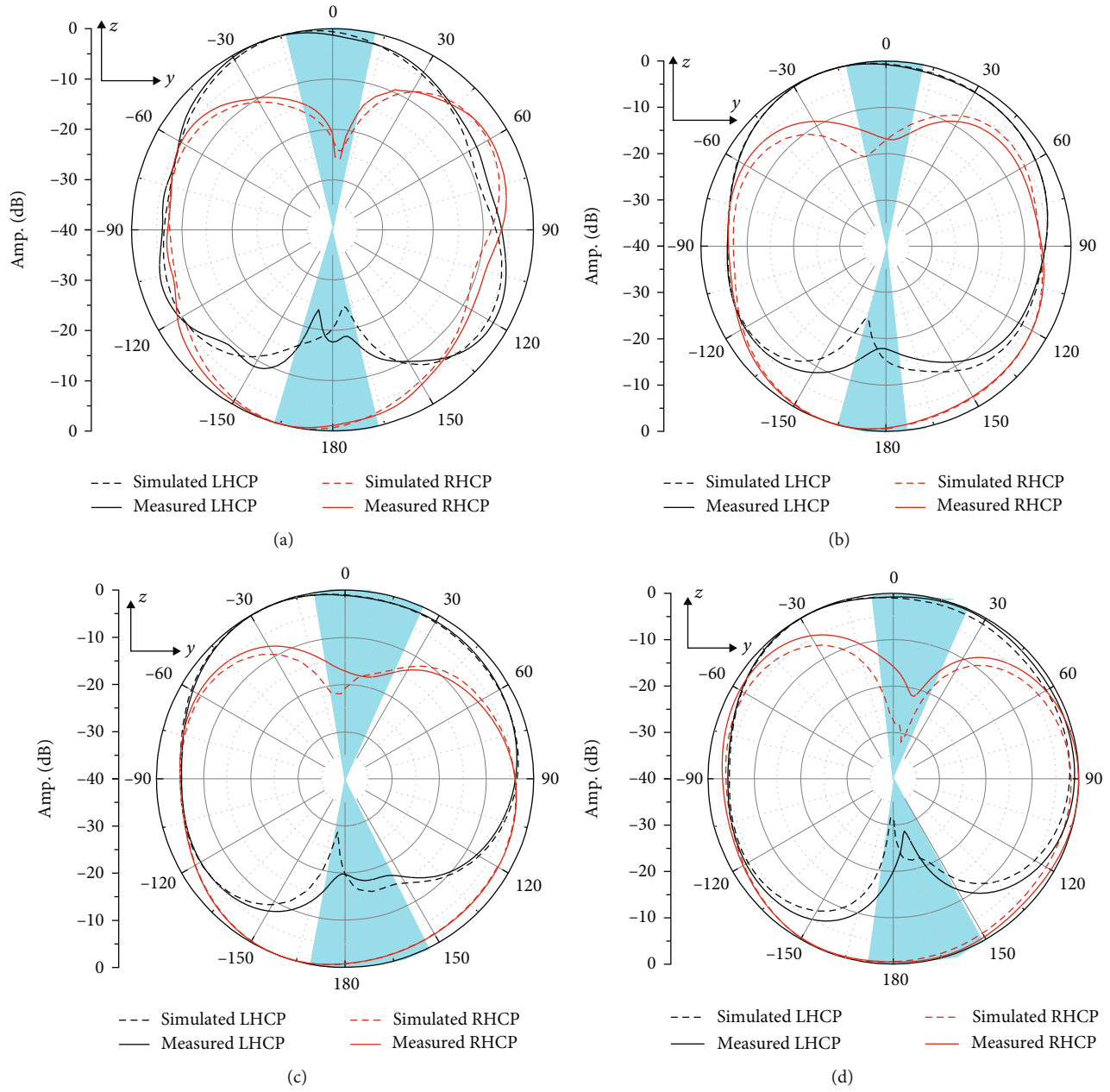

Figure 8: Measured and simulated radiation patterns in zy-plane at (a) 2.40 GHz, (b) 2.52 GHz, (c) 2.60 GHz, and (d) 2.68 GHz.

simulated one. The same situation also applies at another reflection zero resonated at 2.7 GHz, with a discrepancy less than 0.1%. The experimental $|S_{11}| < -10$ dB covers a range from 2.35 to 2.79 GHz, i.e., about 20.1% in fraction, which is extremely consistent with the simulated one (2.35-2.78 GHz, 19.6% in fraction). This implies that a wide dual-mode resonant impedance bandwidth of the proposed slot antenna has been successfully achieved by incorporating a slotline stub. It also can be observed that the measured two minima frequency points of the 3 dB AR response are at 2.44 GHz and 2.68 GHz, with discrepancies less than 1.4% and 0.7%, respectively. More importantly, the tendency resultants of the reflection coefficients and 3 dB AR responses show good agreement. In addition, the measured 3 dB AR bandwidth covers a range from 2.36 to 2.72 GHz (16.3% in fraction), while the simulated one is 2.30-2.76 GHz (20.9% in fraction). As is shown, the measured left minima AR frequency point has slightly moved upward compared with the numerical one, resulting in a 4.6% fall-off in the achievable fractional bandwidth. This is possibly caused by fabrication tolerance of the left distance D_{s1}: as is illustrated in Figure 4(c), larger D_{s1} may yield wider 3 dB AR bandwidths where the left minima AR frequency point shifts to lower frequencies. In general, the measured results once again verify the correctness of the analytical design approach as supported by a set of closed-form design formulas.

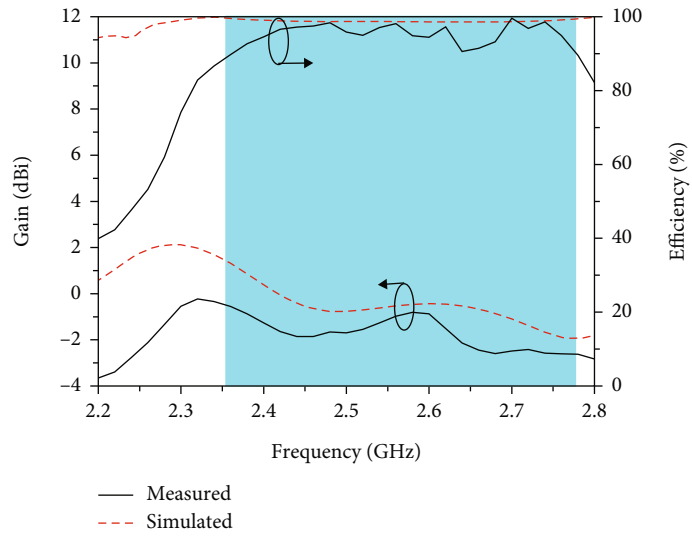

Figure 9: Measured and simulated gains and efficiencies.

Table 2: Comparisons of wideband CP antennas.

Ref.	Number of parameters	Number of ports	Measured impedance BW (%)	Measured 3 dB AR BW (%)	Closed-form design formulas	External phase shift networks/ parasitic elements
[11]	8	1	36.0	19.0	No	Yes
[15]	8	1	6.8	22.4	No	Yes
[18]	14	1	18.5	9.1	No	Yes
[20]	7	1	7.7	32.7	Yes	Yes
[21]	15	1	4.9	35.5	No	Yes
[22]	13	1	7.4	19.7	Yes	Yes
[26]	11	2	8.8	10.3	Yes	Yes
[27]	11	2	5.4	9.3	Yes	Yes
This work	14	1	20.1	16.3	Yes	No

Figures 8(a), 8(b), 8(c), and 8(d) demonstrate the measured and simulated normalized radiation patterns in zy-plane (elevation-plane) at $f = 2.40$, 2.52, 2.60, and 2.68 GHz, respectively. Both measured and simulated normalized radiation patterns match well with each other, and their discrepancies are inevitably caused by errors in fabrication and installation. As is expected, the designed antenna exhibits a left-handed CP radiation pattern in the boresight direction, while a right-handed one in the opposite direction. The measured 3 dB AR bandwidths at higher frequencies in the $+z$- and $-z$-directions (i.e., 30°/37° at 2.68 GHz) are slightly wider than the ones at lower frequencies (i.e., 27°/30° at 2.40 GHz). As can be observed, the main beam has been slightly distorted to a tilted one owing to the asymmetric geometry of the proposed antenna. Figure 9 plots the matched measured and simulated gains and efficiencies within the corresponding impedance bandwidth, whereas the measured efficiency is 95% on average. If a high gain performance is required, the ground plane size of the antenna can be appropriately increased.

Table 2 tabulates the comprehensive comparisons in terms of number of parameters, number of ports, 3 dB AR bandwidth, impedance bandwidth, external phase shift networks/parasitic elements, and closed-form design formulas. Compared to most of the wideband CP antennas [11, 15, 18, 21] which hardly control the number of resonances in the $|S_{11}|$ and axial ratio (AR) frequency responses, the design approach can solve the issues by supporting by a set of closed-form design formulas. More importantly, the advanced antenna should be yielding the simplest, straight-line configuration without external phase shift networks/parasitic elements [11, 15, 18, 20–22, 26–27] and maintain equal length, straight-line configuration of the orthogonal slotline dipoles. Besides, it retains a relatively simple configuration (i.e., single port vs. dual port [26, 27]) and compact size (i.e., lower profile vs. bulky size [19, 20]) to most of its CP counterparts. Since the usable resonant modes can be excited and identified as desired, the resultant antenna exhibits approximately equal wideband AR and impedance bandwidths. These good agreements between the measured and simulated results and the comprehensive comparisons have further evidently validated that the proposed approach as supported by a set of closed-form design formulas should be correct and effective for wideband dual-mode resonant

CP slotline antenna without using external phase shift network.

4. Conclusions

Design approach to a wideband dual-mode resonant open-end slotline antenna is proposed in this article. The resultant stub asymmetry-enabled self-phase-shift CP antenna under dual-mode resonance can automatically realize nearly equal wideband AR bandwidth (up to 16.3%) as wide as impedance bandwidth (up to 20.1%) by incorporating unequal microstrip branches and asymmetrical slotline stubs. The advanced analytical design approach as supported by a set of closed-form formulas can indeed forward predict and estimate the basic configuration and number of usable resonant modes of the conceptual antenna. Therefore, the advanced antenna in this work is expected to be employed to design conformal antennas for vehicular applications [36, 37] while maintaining the simplest, straight-line configuration.

Data Availability

The data used to support the findings of this study are included within the article.

Conflicts of Interest

All authors declare that there is no conflict of interest regarding the publication of this paper.

Acknowledgments

This work was supported by the National Key Research and Development Program of China under grant no. 2021YFE0205900, Key Technologies R&D Program of Jiangsu (Prospective and Key Technologies for Industry) under grants BE2022067 and BE2022067-2, University of Macau under grant CPG202200008-FST, and the Postgraduate Research and Practice Innovation Program of Jiangsu Province under Grant KYCX21_0722.

References

[1] H. Iwasaki, "A circularly polarized small-size microstrip antenna with a cross slot," *IEEE Transaction on Antennas and Propagation*, vol. 44, no. 10, pp. 1399–1401, 1996.

[2] M. F. Bolster, "A new type of circular polarizer using crossed dipoles," *IRE Transactions on Microwave Theory and Techniques*, vol. 9, no. 5, pp. 385–388, 1961.

[3] Y. Xu, S. Gong, and T. Hong, "Circularly polarized slot microstrip antenna for harmonic suppression," *IEEE Antennas and Wireless Propagation Letters*, vol. 12, pp. 472–475, 2013.

[4] L. Zhong, J. S. Hong, and H. C. Zhou, "A dual-fed aperture-coupled microstrip antenna with polarization diversity," *IEEE Transaction on Antennas and Propagation*, vol. 64, no. 10, pp. 4524–4529, 2016.

[5] C. Liu, Y. X. Guo, and S. Xiao, "Circularly polarized helical antenna for ISM-band ingestible capsule endoscope systems," *IEEE Transaction on Antennas and Propagation*, vol. 62, no. 12, pp. 6027–6039, 2014.

[6] X. Tang, Y. He, and B. Feng, "Design of a wideband circularly polarized strip-helical antenna with a parasitic patch," *IEEE Access*, vol. 4, pp. 7728–7735, 2016.

[7] B. Strassner and K. Chang, "5.8-GHz circularly polarized dual-rhombic-loop traveling-wave rectifying antenna for low power-density wireless power transmission applications," *IEEE Transaction on Micro-wave Theory and Techniques*, vol. 51, no. 5, pp. 1548–1553, 2003.

[8] Y. H. Yang, B. H. Sun, and J. L. Guo, "A single-layer wideband circularly polarized antenna for millimeter-wave applications," *IEEE Transaction on Antennas and Propagation*, vol. 68, no. 6, pp. 4925–4929, 2020.

[9] Y. Yao, F. Zhang, and F. Zhang, "Microstrip fed planar endfire circularly polarised antenna with enhanced bandwidth," *Electronics Letters*, vol. 53, no. 7, pp. 445-446, 2017.

[10] P. Mousavi, "Multiband multipolarization integrated monopole slots antenna for vehicular telematics applications," *IEEE Transaction on Antennas and Propagation*, vol. 59, no. 8, pp. 3123–3127, 2011.

[11] D. Yang, H. Li, B. Ren, W. Cao, and R. Huang, "Pin-loaded planar wideband end-fire circularly polarised antenna," *Electronics Letters*, vol. 57, no. 14, pp. 536–538, 2021.

[12] X. Liang, J. Ren, L. Zhang et al., "Wideband circularly polarized antenna with dual-mode operation," *IEEE Antennas and Wireless Propagation Letters*, vol. 18, no. 4, pp. 767–770, 2019.

[13] W. J. Yang, Y. M. Pan, and S. Y. Zheng, "A low-profile wideband circularly polarized crossed-dipole antenna with wide axial-ratio and gain beamwidths," *IEEE Transaction on Antennas and Propagation*, vol. 66, no. 7, pp. 3346–3353, 2018.

[14] Z. H. Tu, K. G. Jia, and Y. Y. Liu, "A differentially fed wideband circularly polarized antenna," *IEEE Antennas and Wireless Propagation Letters*, vol. 17, no. 5, pp. 861–864, 2018.

[15] X. Chen, L. Yang, J. Y. Zhao, and G. Fu, "High-efficiency compact circularly polarized microstrip antenna with wide beamwidth for airborne communication," *IEEE Antennas and Wireless Propagation Letters*, vol. 15, pp. 1518–1521, 2016.

[16] C. F. Zhou and S. W. Cheung, "A wideband CP crossed slot antenna using *1- λ* resonant mode with single feeding," *IEEE Transaction on Antennas and Propagation*, vol. 65, no. 8, pp. 4268–4273, 2017.

[17] M. K. Ray, K. Mandal, N. Nasimuddin, A. Lalbakhsh, R. Raad, and F. Tubbal, "Two-pair slots inserted CP patch antenna for wide axial ratio beamwidth," *IEEE Access*, vol. 8, pp. 223316–223324, 2020.

[18] A. A. Abdulmajid, Y. Khalil, and S. Khamas, "Higher-order-mode circularly polarized two-layer rectangular dielectric resonator antenna," *IEEE Transaction on Antennas and Propagation*, vol. 17, no. 6, pp. 1114–1117, 2018.

[19] R. Kuma, A. Chandra, and D. Chaturvedi, "Wideband circularly polarized rectangular dielectric resonator antenna using inverted U-shaped ground plane for sub 6GHz and upper mid-bands 5G applications," in *In Proceedings of the 2023 Photonics & Electromagnetics Research Symposium (PIERS)*, pp. 2014–2018, Prague, Czech Republic, 2023.

[20] J. F. Lin and Q. X. Chu, "Enhancing gain of ring slot antennas with shorting strips," *IEEE Transaction on Antennas and Propagation*, vol. 67, no. 7, pp. 4397–4405, 2019.

[21] J. Li, J. Shi, L. Li et al., "Dual-band annular slot antenna loaded by reactive components for dual-sense circular polarization with flexible frequency ratio," *IEEE Access*, vol. 6, pp. 64063–64070, 2018.

[22] Y. Xu, L. Zhu, and N. W. Liu, "Design approach for a dual-band circularly polarized slot antenna with flexible frequency ratio and similar in-band gain," *IEEE Antennas and Wireless Propagation Letters*, vol. 21, no. 5, pp. 1037–1041, 2022.

[23] W. He, Y. He, S. W. Wong, and C. H. Liao, "A wideband circularly polarizedS-shaped slot antenna," *International Journal of RF and Microwave Computer-Aided Engineering*, vol. 31, no. 5, Article ID e22612, 2021.

[24] R. Xu, J. Li, Y. X. Qi, Y. Guangwei, and J. J. Yang, "A design of triple-wideband triple-sense circularly polarized square slot antenna," *IEEE Antennas and Wireless Propagation Letters*, vol. 16, pp. 1763–1766, 2017.

[25] M. S. Ibrahim, "Low-cost, circularly polarized, and wideband U-slot microstrip patch antenna with parasitic elements for WiGig and WPAN applications," in *Proceedings of the 2019 13th European Con-ference on Antennas and Propagation (EuCAP)*, Krakow, Poland, 2019.

[26] Q. S. Wu, X. Zhang, and L. Zhu, "Co-design of a wideband circularly polarized filtering patch antenna with three minima in axial ratio response," *IEEE Transaction on Antennas and Propagation*, vol. 66, no. 10, pp. 5022–5030, 2018.

[27] Q. S. Wu, X. Zhang, and L. Zhu, "A wideband circularly polarized patch antenna with enhanced axial ratio bandwidth via co-design of feeding network," *IEEE Transaction on Antennas and Propagation*, vol. 66, no. 10, pp. 4996–5003, 2018.

[28] X. H. Mao, W. J. Lu, F. Y. Ji, X. Q. Xing, and L. Zhu, "Dual radial-resonant wide beamwidth circular sector microstrip patch antennas," *Chinese Journal of Electronics*, vol. 32, no. 4, pp. 710–719, 2023.

[29] J. Zhang, W. J. Lu, L. Li, L. Zhu, and H. B. Zhu, "Wideband dual-mode planar endfire antenna with circular polarisation," *Electronics Letters*, vol. 52, no. 12, pp. 1000-1001, 2016.

[30] L. Li, J. Zhang, W. J. Lu, W. H. Zhang, and L. Zhu, "Dual-mode planar end-fire circularly polarized antenna," in *Proceedings of the 2016 IEEE International Workshop on Electromagnetics: Applications and Student Innovation Competition (iWEM)*, Nanjing, China, 2016.

[31] W. J. Lu and L. Zhu, "Wideband stub-loaded slotline antennas under multi-mode resonance operation," *IEEE Transaction on Antennas and Propagation*, vol. 63, no. 2, pp. 818–823, 2015.

[32] W. J. Lu, L. Zhu, K. W. Tam, and H. B. Zhu, "Wideband dipole antenna using multi-mode resonance concept," *International Journal of Microwave and Wireless Technologies*, vol. 9, no. 2, pp. 365–371, 2017.

[33] W.-J. Lu, "Generalized odd-even mode theory and mode synthesis antenna design approach," *Electromagnetic Science*, 2024, in press.

[34] L. Zhu, R. Fu, and K. L. Wu, "A novel broadband microstrip-fed wide slot antenna with double rejection zeros," *IEEE Antennas and Wireless Propagation Letters*, vol. 2, pp. 194–196, 2003.

[35] R. Garg, P. Bhartia, I. Bahl, and A. Ittipiboon, *Microstrip Antenna Design Handbook*, Artech House, Boston, 2001.

[36] H. Zhao, F. Ge, Q. Zhang, S. Li, and X. Yin, "Asymmetric end-fire frequency scanning tapered slot antenna with spoof surface plasmon polaritons," *IEEE Transaction on Antennas and Propagation*, vol. 70, no. 7, pp. 5913–5917, 2022.

[37] W. A. Johnson, "The notch aerial and some applications to aircraft radio installations," *Proceedings of the IEE-Part B: Radio and Electronic Engineering*, vol. 102, no. 2, pp. 211–218, 1955.